Molecular Crystals and Liquid Crystals
Publication details, including instructions for authors and subscription information:
http://www.tandfonline.com/loi/gmcl20

Optical Manipulation of Liquid Crystal Droplets Through Holographic Polarized Tweezers: Magnus Effect

J. Hernández [a], C. Provenzano [a], P. Pagliusi [a b] & G. Cipparrone [a b]
[a] Physics Department, University of Calabria, 87036, Rende-CS, Italy
[b] IPCF-CNR, UOS Cosenza and Excellence Centre CEMIF.CAL, University of Calabria, 87036, Rende-CS, Italy
Version of record first published: 18 Apr 2012.

To cite this article: J. Hernández , C. Provenzano , P. Pagliusi & G. Cipparrone (2012): Optical Manipulation of Liquid Crystal Droplets Through Holographic Polarized Tweezers: Magnus Effect, Molecular Crystals and Liquid Crystals, 558:1, 72-83

To link to this article: http://dx.doi.org/10.1080/15421406.2011.653712

Mol. Cryst. Liq. Cryst., Vol. 558: pp. 72–83, 2012

ISSN: 1542-1406 print/1563-5287 online
DOI: 10.1080/15421406.2011.653712

Taylor & Francis
Taylor & Francis Group

Optical Manipulation of Liquid Crystal Droplets Through Holographic Polarized Tweezers: Magnus Effect

J. HERNÁNDEZ,[1,*] C. PROVENZANO,[1] P. PAGLIUSI,[1,2] AND G. CIPPARRONE[1,2]

[1]Physics Department, University of Calabria, 87036 Rende-CS, Italy
[2]IPCF-CNR, UOS Cosenza and Excellence Centre CEMIF.CAL, University of Calabria, 87036 Rende-CS, Italy

We investigate the manipulation and trapping features of polarization holographic tweezers with liquid-crystal (LC) droplets in water. The force related to light's polarization pattern translates isotropic particles, while for birefringent particles exert forces and torques in opposite directions depending on the position of the particle. Experiments with LC emulsions allow verify expected scenarios and observe unconventional trapping of spinning birefringent particles in circularly-polarized fringes. This unusual trapping featured by rotating-bipolar-droplets suggest the involvement of one hydrodynamic force or Magnus Effect at low Reynolds number. This result shows that Magnus force contributes to opto-hydrodynamic trapping and is demonstrated with an experiment.

Keywords Liquid crystals; magnus Effect; optical trapping; polarization holography

Introduction

An optical trap is an instrument of manipulation and analysis based on an intensity gradient usually called optical tweezers [1]. The gradient of light combined with additional forces due to light scattering and gravity, creates a stable trap position close to the focal point of the beam that draws dielectric (transparent) particles towards the focus. This conventional trapping operation allow to capture microparticles and stably manipulate, while the medium (usually water) yields a damping effect through the viscous force, thus facilitating the experimental study of small particles in many research fields [1–7]. Recently, the use of polarization patterns has demonstrated new trapping and manipulation capabilities based on polarization gradients [8]. The polarization holography relies on the interference of asymmetrically polarized beams [9–11]. Here we report two experiments to ascertain the capabilities for optical trapping and manipulation based on holographic polarization traps. Further details are presented in the following sections where elliptical modulated polarization (Sec. I) and circular polarization (Sec. II) are studied separately. In the first one, a polarization gradient connected with a modulation of the ellipticity and uniform intensity shows an optical force related to the polarization of light that can influence

*Address correspondence to J. Hernández, Physics Department, University of Calabria, 87036 Rende-CS, Italy. E-mail: josueraul.hernandez@fis.unical.it

optically isotropic particles, whereas in the case of birefringent particles an unconventional trapping in circularly polarized fringes is observed. In the second one, to demonstrate the effect of the Magnus force we devised an experiment of optical micromanipulation. The experiment exploits a holographic optical trap based on the interference of two laser beams with parallel circular polarization to set in rotation a particle and drag it in the fluid.

Experimental

The experimental set-up used for laser trapping, optical forces and torques on droplets is depicted in Fig. 1(a). An argon laser beam at $\lambda = 488$ nm is directed towards a Mach-Zehnder interferometer and directed inside a microscope objective to interfere on the sample. In the first experiment, the beams at the exit of the objective 60X (NA = 0.85) have orthogonal *s* and *p* linear polarizations using a half-wave-plate (HWP) before BS2 [Fig. 1(a)]. The diameters for both beams entering the objective and the illuminated area of the sample were 2 mm and 40 μm, respectively. The intensity in the interference region was uniform ($\sim$100 mW/cm^2) and the spatial periodicity of the polarization pattern $\Lambda \sim 10$ μm [Fig. 1(b)]. In the second experiment we used a different objective lens 40X (NA = 0.65) and removed the HWP, to obtain parallel circular polarization state an additional quarter-wave-plate was introduced before the objective. The total power of the laser beam was $P_0 \approx 100$ mW with a spot size in the interference pattern of $\omega_0 \sim 100$ μm; the spatial periodicity was $\Lambda \sim 10$ μm. In both experiments, a piezoelectric actuated mirror mount, electrically driven by a function generator, allowed the controlled movement of the mirror M1 of the Mach-Zehnder interferometer to translate the interference light fringes. The measurements were performed displacing the interference pattern with a sinusoidal time modulated function.

The samples employed were emulsions of nematic liquid crystal (LC) E7 in distilled water, a system already adopted for optical manipulation experiments [12,13]. A relevant aspect of this system is that droplets with radial and bipolar nematic configuration, can be found in the same emulsion [13]. Spherical droplets of nematic liquid crystal with diameter ranging from 1 μm to 20 μm can be obtained and are transparent in the whole visible range, with radial or bipolar configuration of the nematic director [8,12,13].

Results and Discussion

I. Elliptical Modulated Polarization

In this case, we considered the interference of two beams with orthogonal linear polarizations *s* and *p*, both having the same intensity and crossing at a small angle, see Fig 1(b). The choice of this pattern relies on the peculiarity that no intensity modulation occurs in the interference region and the purely vectorial polarization pattern consists of an elliptical polarization of constant inclination ($\pm 45^\circ$), whose ellipticity is continuously modulated from -1 to 1 along the x-coordinate, see Fig. 1(b).

The resulting optical electric field and intensity profile in an homogeneous and isotropic medium were respectively [9,10]

$$\vec{E}_{s,p} = E_o\Big(\cos\frac{\theta}{2}\exp(-i\delta)\hat{x} + \exp(i\delta)\hat{y} - \sin\frac{\theta}{2}\exp(-i\delta)\hat{z}\Big)\exp(-i\beta)$$

$$I_{s,p} = 2E_0^2 \quad (1)$$

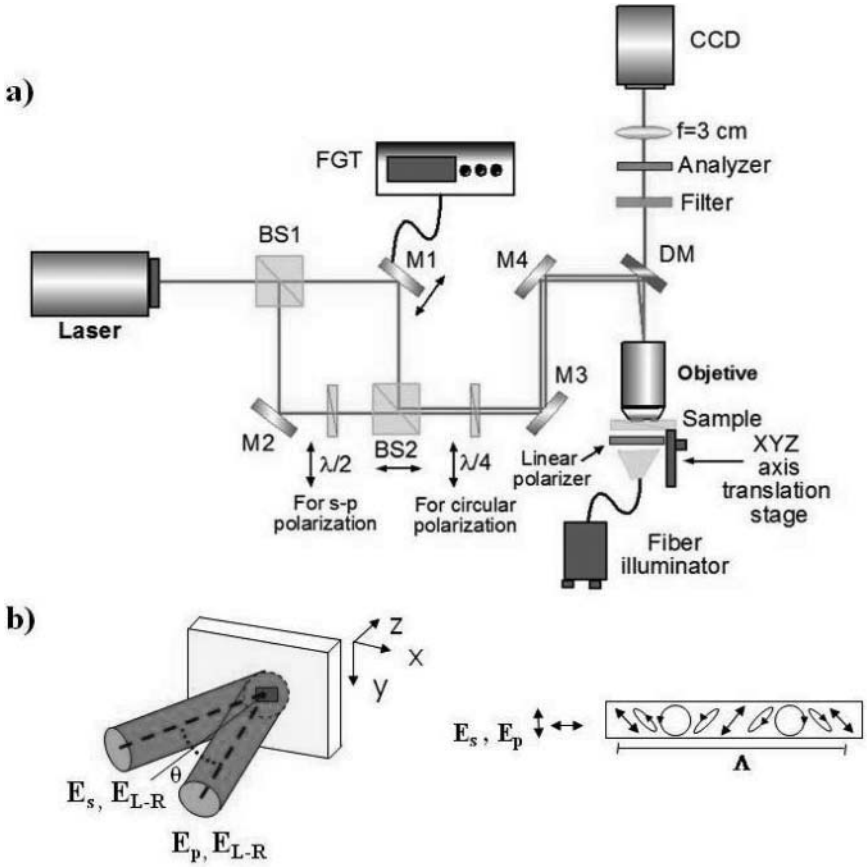

Figure 1. (a) Experimental set up. A *s*-polarized Argon ion laser beam at $\lambda = 488$ nm, is sent into a Mach-Zehnder interferometer. The two beams are directed towards the (40X for s-p) 60X microscope objective through a dichroic mirror (DM), focusing the resulting polarization interference pattern on the sample. For *s-p* polarization the half-wave plate ($\lambda/2$), changes the state of one light beam to have orthogonal linear polarization. The quarter-wave plate ($\lambda/4$), changes the polarization state of the light beams from linear to circular [both left (L) or both right (R)]. The spatial periodicity of the fringes can be tuned by shifting the beam splitter BS2. The mirror M1 is mounted on a piezoelectric system, driven by an arbitrary function generator, and enables the movement of the fringes. M2, M3 and M4 are fixed mirrors. The sample position is adjusted via a three-axis translation stage. A computer controlled CCD camera and a fibre illuminator have been used to image the sample. (b) Representation of the two beams with orthogonal linear polarizations *s* and *p* (or circular parallel *L-L* or *R-R*), both having the same intensity and crossing at a small angle.

where n is the refractive index, $\beta = \frac{2\pi n}{\lambda}\cos\frac{\theta}{2}z$, $\delta = \frac{2\pi n}{\lambda}\sin\frac{\theta}{2}x = \frac{\pi}{\Lambda}x$ and $\Lambda = \frac{\lambda}{2n\sin\theta/2}$ is the spatial periodicity of the pattern. To evaluate the mechanical properties of such light fields, the linear and angular momentum densities were calculated. The linear momentum density carried by the light in the interference region was given by:

$$\vec{g} = \frac{1}{c^2}\mathrm{Re}\{\vec{E}^* \times \vec{H}\} \tag{2}$$

Evaluating the magnetic fields in the interference region for both cases from the Eq. (1) and (2) respectively, the linear momentum density was:

$$\vec{g}_{p,s} = \frac{1}{c^2}\sqrt{\frac{\varepsilon}{\mu}}E_0^2\left[\left(\sin\theta\cos\frac{2\pi x}{\Lambda}\right)\hat{y} + \left(2\cos\frac{\theta}{2}\right)\hat{z}\right] \tag{3}$$

For linear orthogonal interfering beams, besides the usual longitudinal z-component, an additional transverse y-component occurs for $\vec{g}$, which is spatially modulated versus the x-coordinate along with the polarization pattern (see Fig. 2(a)), and was responsible for the transverse force field along $\hat{y}$ (see Fig. 2(b)). The angular momentum density follows from the linear momentum density as [14]:

$$\vec{j} = \vec{r} \times \vec{g} \tag{4}$$

Then, in the case of linear s and p interference only a z modulated component is present:

$$j_z = \frac{1}{c^2}\sqrt{\frac{\varepsilon}{\mu}}E^2(\sin\theta)\,x\cos\frac{2\pi x}{\Lambda} \tag{5}$$

The total angular momentum J_z, obtained by the integration of j_z over the interference region, exhibits two contributions: the orbital component associated with the spatial distribution of the wave and the spin component associated with the ellipticity of light. When a particle is located in the optical field (1), there is a transfer of linear and angular momentum from light to matter depending on the particle position, shape and size. Therefore the optical

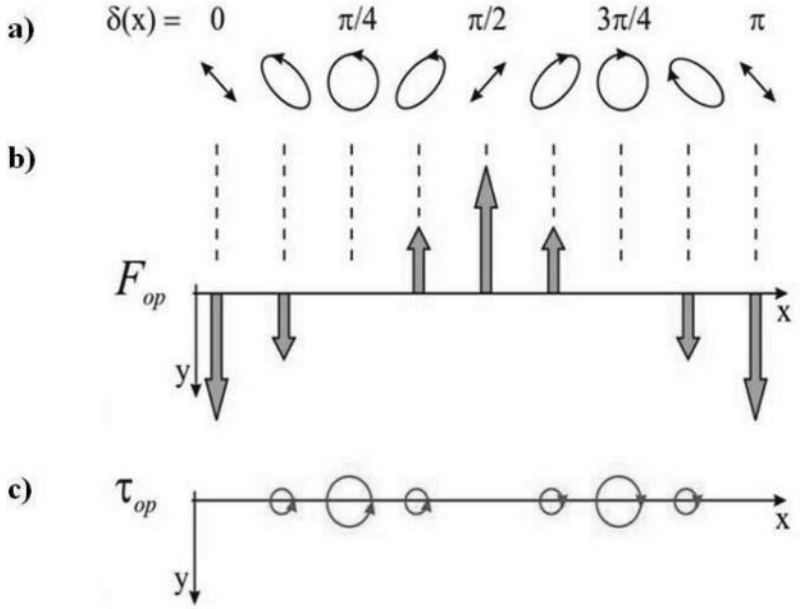

Figure 2. (a) Scheme of the polarization pattern versus the half phase difference $\delta(x)$. (b) Diagram of modulation of the optical force F_{op} (arrows) felt by a particle with diameter lower than $\Lambda/2$. (c) Optical torque τ_{op} (circles) on the spinning particle when is trapped in an interference fringe and is translated along the grating wave along $\hat{x}$.

force

$$\vec{F}_{op} = Q\frac{2A}{c}\left[\hat{y}\sin\theta\iint\cos\frac{2\pi x}{\Lambda}dxdy + \hat{z}2\cos\frac{\theta}{2}\iint dxdy\right] \tag{6}$$

and torque

$$\vec{\tau}_{op} = Q'\frac{2A}{c}\hat{z}\sin\theta\iint x\cos\frac{2\pi x}{\Lambda}dxdy \tag{7}$$

arises over the particle in the xy-plane, where Q and Q' are the parameters accounting for the linear and angular momentum transferred to the particle and A is the intensity of the light.

Only the optical linear momentum can be transferred to radial droplets, which are optically isotropic with an average refractive index higher than that of water. On the other hand, both linear and angular momentum can be transferred to bipolar droplets, which are optically anisotropic. These features enable to test different dynamical behaviors, maintaining almost constant the experimental conditions and the materials parameters, i.e. the average refractive index of the droplets and their diameter in the range of 2–5 μm ($d \leq \Lambda/2$).

To test the mechanical properties of the light polarization pattern resulting from the interference of s and p linear polarization, we firstly consider the effect on a transparent isotropic radial LC droplet, at rest in a circular polarization fringe. No transfer of angular momentum occurs ($\vec{\tau}_{op} = \vec{0}$) implying null angular velocity $\vec{\Omega}$. The translation of the polarization pattern induces a displacement of the particle along $\pm\hat{y}$, due to the birth of the $F_{op,y}$ [Fig. 3]. The droplets experienced the modulated components of the optical force, with a calculated amplitude 0.1–1 pN, according to Eq. (6).

When an optically anisotropic particle, i.e. a bipolar droplet, is placed in a circular polarization fringe, due to the transfer of the angular momentum spin ($\vec{\tau}_{op} \neq 0$), it is set in rotation [12]. The uniform angular velocity ($\vec{\Omega} = \text{const.}$) satisfies the condition $\vec{\tau}_D + \vec{\tau}_{op} = \vec{0}$, where $\vec{\tau}_D = -8\pi\eta a^3\vec{\Omega}$ is the viscous torque, a is the radius of the particle and η the fluid viscosity. The measured rotation frequency values were a few Hz (2–5 Hz). In this case, the translation of the polarization pattern induced an unconventional trapping of the spinning particle in the fringe, dragging it along $\pm\hat{x}$. The Fig. 4 shows the trapping of a bipolar droplet rotating clockwise in a circular polarization fringe. The shift of the polarization

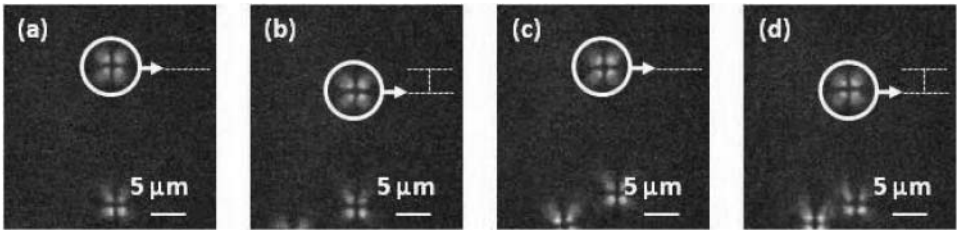

Figure 3. Image showing the maximum displacement of an optically isotropic (i.e., radial) LC droplet due to the movement of the polarization pattern. For a non-rotating particle, only the optical force F_{op} occurs. Frames (a)–(d) show the droplet displacement along the y-axis induced by the spatially modulated $F_{op,y}$. The LC droplet moves up and down by ~2 mm depending on the $F_{op,y}$ direction [See Fig. 2(b)].

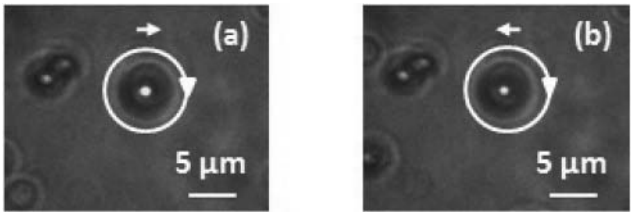

Figure 4. Dynamics of an optically anisotropic (bipolar) LC droplet by shifting the polarization pattern. (a) The lift force traps the rotating particle in the circular polarization fringes and without displacement along the *y* direction. (b) Similar behaviour is observed when the sample is translated with respect to the polarization pattern.

pattern along $-\hat{x}$ does not showed a displacement of the droplet along $\pm\hat{y}$ and the droplet preserved the clockwise rotation, see Fig. 4.

The experimental findings for the isotropic, non-rotating, LC droplets verified how the polarization nature of the light influences isotropic particles through the vectorial holography; confirming the effect of the optical force coming from the polarization gradient, see Eq. (6). On the other hand, the trapping of the anisotropic particles in the circular polarization fringes, when they are set in rotation by the optical torque (7), cannot be accounted by the mere optical force because of its null x-component. Moreover, even considering the momentum redistribution of the light after passing through the rotating birefringent droplet, the calculated optical force did not exhibit any *x*-component, which might justify the observed behavior. To explain the observed unusual trapping we reconsider the influence of the ambient fluid on the particle dynamics and their consequences on the trapping and manipulation performances, for this reason the holographic tweezers studied in our experiment were based on a more gentle approach to the usual optical manipulation, as a consequence the effect of possible hydrodynamics forces on the particles should not be neglected as will be show in the next section.

II. Parallel Circular Polarization: Magnus Effect

A complete study of the dynamics of the LC droplets in an optical field requires to consider the equations of motion of spherical particles in a viscous fluid, including the hydrodynamic forces and torques. The areas of study and applications that have mainly addressed the experiments and the theoretical modeling until now refer to situations in which the particles are suspended in shear and vortical flows and where the Reynolds number (Re) involved is high or moderated [15–18]. The systems typically used for optical trapping, exhibit strongly viscous behavior governed by Stokes equations, and refer to a small Reynolds number regime [19]. Only a few old papers have studied the motion of particles in a fluid at small Reynolds number, which is the case encountered in optical manipulation experiments. Rubinow and Keller [19] evaluated the resultant force on a spinning spherical particle moving with initial linear and angular velocity in a static viscous fluid. Solving the Navier-Stokes equations, they found that in addition to the drag force, a spinning particle experiences a force orthogonal to the direction of motion given by:

$$\vec{F}_M = \pi R^3 \rho \vec{\Omega} \times \vec{v} \left[1 + O(\mathrm{Re})\right], \tag{8}$$

known as lift force or Magnus force, where R is the radius of the spherical particle, $\vec{\Omega}$ its angular velocity, $\vec{v}$ its linear velocity, $\mathrm{Re} = \rho v R/\eta$ the Reynolds number with ρ and η as the density and the viscosity of the fluid, respectively. This force is originated from the different velocity of the fluid on the opposite sides of the particle due to the vortices in the ambient flow or due to the rotation of the particles in the shear flow, acting perpendicularly to the slip velocity. In a different work, Saffman considered the lift force on a small sphere in a slow shear flow [20], in the theoretical models reported in these papers is stated that in the case of micrometric particles at low Reynolds number where $\mathrm{Re} < 1$ and $R \sim 10^{-6}$ m, the Magnus force can be neglected with respect to the drag (or viscous) force. For this reason, the researchers working in the field of optical manipulation have always ignored this force. However, we noted that the situations considered by the theoretical studies on the Magnus force do not reflect the conditions of the optical micromanipulation experiments, where an external agent (i.e., the light) rotates and/or translates the particles in a static fluid. For this reason, adopting a simple modelling approach and a trajectory method [21], we proof and evaluate the Magnus force in an experimental condition, showing that it is unexpectedly much larger than the one predicted by the existing theories and therefore, cannot be neglected in the case of spinning micrometric particles at low Reynolds number.

The experiment uses a holographic optical trap based on a simple interference pattern of two beams with parallel circular polarization. The resulting light pattern performed one dimensional optical trapping within the light interference fringes [8]; while the light pressure in the longitudinal direction ($\hat{z}$) and the gradient force along the light stripes ($\hat{y}$) were weak. The resultant intensity on the interference pattern from the beams with spatial periodicity Λ in the plane (x, y), is expressed as:

$$I = \frac{4P_0}{\pi w_0^2} \cos^2\left(\frac{\pi}{\Lambda}x\right) \exp\left(-\frac{2(x^2+y^2)}{w_0^2}\right), \tag{9}$$

where P_0 is the total light power and w_0 is the Gaussian spot size of the beams.

In a very simple approach adequate for a microscopic object, the dipole moment induced in the particle responds to field gradients, yielding to a force proportional to the intensity gradient and then the optical force can be written as:

$$\vec{F}_{op} = D\left\{\left[-\frac{\pi}{\Lambda}\sin\left(\frac{2\pi x}{\Lambda}\right) - \frac{4x}{w_0^2}\cos^2\left(\frac{\pi}{\Lambda}x\right)\right]\exp\left(-\frac{2(x^2+y^2)}{w_0^2}\right)\right\}\hat{x}$$
$$+ D\left\{\left[-\frac{4y}{w_0^2}\cos^2\left(\frac{\pi}{\Lambda}x\right)\right]\exp\left(-\frac{2(x^2+y^2)}{w_0^2}\right)\right\}\hat{y} \tag{10}$$

where $D = (2\pi R^3/c)\, n_f\, \{[(n_p/n_f)^2-1]/[(n_p/n_f)^2+2]\}(4P_0/w_0^2)$, n_p and n_f are the refractive indices of the particle and the fluid, respectively. The x component of the optical force is dominated by the term $\sim sin\,(2\pi\,\mathrm{x}/\Lambda)$, which exhibits the same spatial periodicity Λ as the interference pattern in Eq. (9), but phase shifted by $\Lambda/4$, enabling the trapping in the bright fringes [Fig. 5].

According to the experimental scheme, we describe the motion of the trapped particle starting from the set of equations of the motion of a spherical particle in an isotropic fluid,

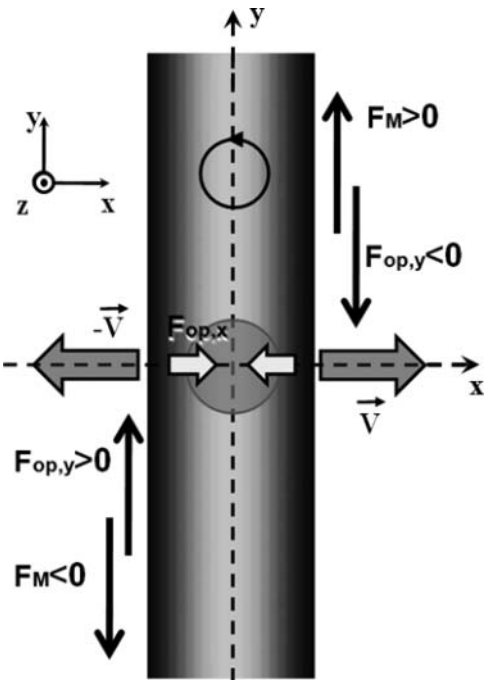

Figure 5. Scheme of the forces acting on the spinning particle anticlockwise when is trapped in an interference fringe and is translated along the grating wave vector direction, i.e. perpendicularly with respect to the light fringe along $\hat{y}$. The directions of the forces, optical force F_{op} and Magnus force F_M, along the y axis are sketched in the case of a movement along $\hat{x}$ or $-\hat{x}$ with linear velocities $\vec{V}$ and $-\vec{V}$, respectively.

subjected to the optical force and torque:

$$m\frac{d\vec{v}}{dt} = \vec{F}_D + \vec{F}_M + \vec{F}_{op}, \tag{11}$$

$$I\frac{d\vec{\Omega}}{dt} = \vec{\tau}_D + \vec{\tau}_{op}, \tag{12}$$

where m is the mass of the sphere and I the moment of inertia. $\vec{F}_D = -b\vec{v}$ is the viscous force, with $b = 6\pi R\eta$ in the case of a spherical particle and $\vec{\tau}_D$ and $\vec{\tau}_{op}$ are the viscous and optical torques. $\vec{F}_M = C_M\rho\vec{\Omega} \times \vec{v}$ is the Magnus force experienced by a particle rotating with angular velocity $\vec{\Omega}$ and translating with linear velocity $\vec{v}$ within a static fluid, C_M is a parameter related to the physical and geometrical features of the particle. Again as the previous section, we consider the case of particles spinning at a constant angular velocity $\vec{\Omega}$ and the translational motion of the particle along the fringes can be described by the equation (11).

In Fig. 5 we report the optical and Magnus forces acting of a spinning particle within an interference fringe to show the combination of the trapping and translational effects. The trajectories of the particle's motion were depicted for all signs of constant linear and angular velocities, in the case of a non-negligible effect of the Magnus force.

The trapped particle was forced to move in the x direction together with the fringe according to the sinusoidal function $x(t) = A\sin(\omega t)$, where A is the amplitude of the oscillatory displacement and ω is the pulsation. Therefore, the x component of the linear velocity of the particle $v_x(t) = A\omega\cos(\omega t)$is an independent parameter. The projection on the y direction for the Eq. (11) is:

$$m\frac{dv_y}{dt} = -bv_y + F\cos(\omega t) - Ky \tag{13}$$

where the y component of the optical force $F_{op,y} = -Ky$ was derived from equation (10) truncated to the first linear term, and can be considered as a simple restoring force with K including all the geometrical and physical parameters of the equation (10); the Magnus force $F_{M,y} = F\cos\omega t$ acts as sinusoidal driving force, written as

$$F = C_M\rho\Omega A\omega. \tag{14}$$

The Eq. (13) describes the motion of a classical forced and damped harmonic oscillator. The steady state solution of Eq. (13) is: $y(t) = Y_0\sin(\omega t + \varphi)$, where the maximum displacement Y_0 is related to the amplitude of the driving (Magnus) force by the following expression:

$$Y_0 = \frac{F}{\sqrt{(K - m\omega^2)^2 + b^2\omega^2}}, \tag{15}$$

The phase shift between the y and x components of the displacement is $\varphi = arctan[b\omega/(K\text{-}m\omega^2)]$.

Figures 6a and 6b show the displacement of a birefringent LC droplet with a diameter of ~5 μm, rotating in an anticlockwise direction ($\vec{\Omega} > 0$) with angular speed of ~30 rad/s when the droplet trapped is sinusoidally dragged to left (6a) and to right (6b) with amplitude

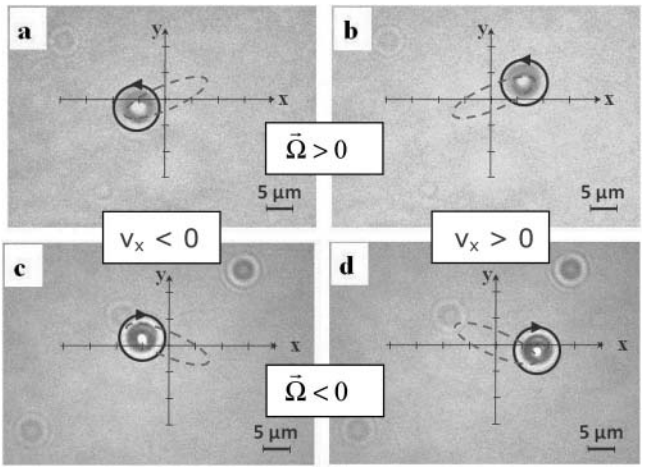

Figure 6. Maximum displacement of the spinning droplet along the y direction in the case of a droplet rotating in an anticlockwise sense ($\vec{\Omega} = \Omega\hat{z}$, $\Omega > 0$) [(a) and (b)]; and for clockwise rotation ($\Omega < 0$) [(c) and (d)], when the translation of the particle is along $-\hat{x}$ corresponding to v < 0 [(a) and (c)] or $\hat{x}$, corresponding to v > 0 [(b) and (d)]. The dashed ellipses indicate the trajectory of the movement followed by the particle.

A = 10 μm and pulsation $\omega \sim 1.6$ rad/s. The displacement of the spinning particle to the left ($v_x < 0$) and to the right ($v_x > 0$) is associated with a correlated downward (6a) and upward (6b) displacement along the y direction, respectively. In Figs. 6c and 6d the displacements of a droplet rotating with opposite angular velocity (i.e., clockwise $\vec{\Omega} < 0$), are in correspondence with $v_x < 0$ and $v_x > 0$. The observed shifts along the y axis are reversed with respect to $\vec{\Omega} > 0$ (see also Fig. 5). The LC droplets with radial director configuration do not rotate in circularly polarized light; therefore no displacement along the y axis is observed even if they are trapped in the fringes and dragged along the x axis.

The values of physical and geometrical parameters of the media and of the light field involved in the experiment were: the mass of the LC droplet, $m \approx 10^{-13}$ kg; the mean refractive index of the liquid crystal (E7), $n_p \approx 1.63$; the refractive index of the water, $n_f = 1.33$; the viscosity of the water, $\eta \approx 10^{-3}$ Ns/m^2; the total power of the laser beams, $P_0 \approx 100$ mW; the spot size of the interference pattern, $w_0 \approx 100$ μm; the spatial periodicity $\Lambda \approx 10\,\mu m$. Considering these experimental data, the calculated values of b and K have the same order of magnitude, $10^{-8}\,Nm^{-1}s$ and $10^{-8}\,Nm^{-1}$ respectively. According to equation (15), the order of magnitude of the Magnus force $F \sim 10^{-14}$ N has been estimated measuring a y-displacement $Y_0 \sim 1$ μm in Figs. 6a–b. The observed particle dynamic yields proof of the Magnus effect and also explain the observed unusual trapping (acting as restoration force) for the case of spinning-bipolar-nematic droplets [See Fig. 7]. We tested several diameters of particles and spatial periodicity of the fringes, but the best configuration was obtained with ($d \leq \Lambda/2$), also testing different host medium (like ethanol and water with soap) to change the viscosity of the fluid the observations were very similar to establish an improvement. Our results show that the Magnus force is at least two orders of

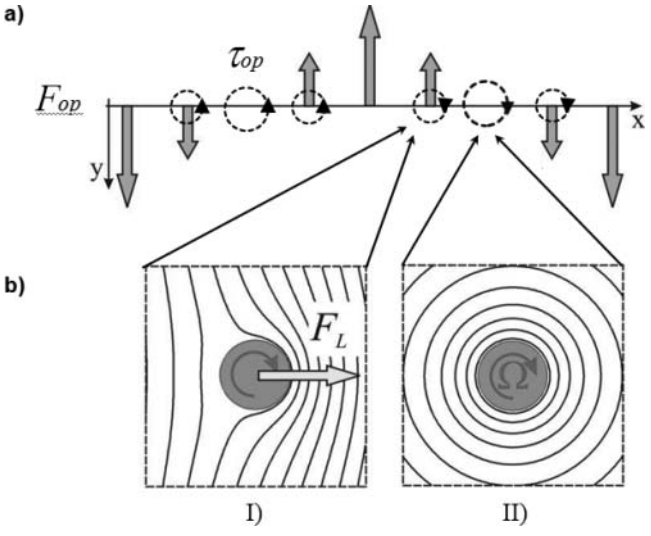

Figure 7. (a) Representation of the optical torque τ_{op} (dashed circles) and the y-component of the optical force F_{op} (vertical arrows) felt by a spherical particle with diameter lower than $\Lambda/2$. (b) [I] Symmetric streamlines occur around the particle, rotating with angular velocity Ω, when it is centred on the circularly polarized fringe. [II] Asymmetric streamlines occur when the particle is centred on an elliptically polarized fringe, due to its linear velocity along the y-axis, and the lift force F_L arises along the x-axis, working as a restoring force for the rotating particle toward the regions with circular polarization.

magnitude larger than the values predicted in the reported theories [19,20]. We consider this discrepancy is due to the fact that theoretical hydrodynamic is too complex and the several approaches to model the movement of spinning microparticles at low Reynolds number do not reflect the experimental conditions. Also, one difference between the reported theory and the present experiment is that in the case of micromanipulation, the constant rotation and translation of the particles are forced by an external field (i.e., the optical field), instead of the free-spinning-particle approach given by theoretical models.

Conclusion

We report the experimental investigation of mechanical properties with polarization patterns. The obtained results show that new strategies for optical trapping and manipulation can be established. Multiple and multifunctional optical traps inside a uniformly illuminated region can be created exploiting the polarization gradient. Two simple experiments have been used to investigate the features of the polarization holographic tweezers. The first experiment, i.e. interference of two linearly orthogonally polarized beams, is the more clear configuration, since no intensity modulations occurs in the superposition region, while the ellipticity is strongly spatially modulated, changing from -1 to 0 and 1. Interesting optical manipulation features for isotropic particles emerge, as well as an unusual hydrodynamic trapping force for birefringent spinning particles. In the second experiment and analysis, a simple modelling approach and a trajectory method have been devised to evaluate the Magnus force, the experiment yields towards unequivocal evidences of the Magnus effect, were only spinning particles show a deviation with respect to the direction of the fringe displacement, the displacement of particles trajectories depends on the signs of their linear and angular velocities. The measurement of the maximum transversal displacement of the rotating particle enables to proof and evaluate the Magnus force in an experimental condition, showing that it is at least two orders of magnitude larger than the one predicted by the existing theories and therefore, cannot be neglected in the case of spinning micrometric particles at low Reynolds number.

References

[1] Ashkin, A., Dziedzic, J. M., Bjorkholm, J. E., & Chu, S. (1986). *Opt. Lett.*, *11*, 288.
[2] Jonas, A., & Zemanek, P. (2008). Light at work: The use of optical forces for particle manipulation, sorting, and analysis. *Electrophoresis*, *28*, 4813.
[3] Grier, D. G. (2003). A revolution in optical manipulation. *Nature*, *424*, 810.
[4] Moffitt, J. R., Chemla, Y. R., Smith, S. B., & Bustamante, C. (2008). Recent advances in optical tweezers. *Ann. Rev. Biochem.*, *77*, 205–228.
[5] Friese, M. E. J., Nieminen, T. A., Heckenberg, N. R., & Rubinsztein-Dunlop, H. (1998). Optical alignment and spinning of laser-trapped microscopic particles. *Nature 394*, 348–350.
[6] Garcès-Chavez, V., McGloin, D., Melville, H., Sibbett, W., & Dholakia, K. (2002). Simultaneous micromanipulation in multiple planes using a self-reconstructing light beam. *Nature*, *419*, 145–147.
[7] Roichman, Y., Sun, B., Roichman, Y., Amato-Grill, J., & Grier, D. G. (2008). Optical forces arising from phase gradients. *Phys. Rev. Lett.*, *100*, 013602.
[8] Cipparrone, G., Ricardez Vargas, I., Pagliusi, P., & Provenzano, C. (2010). Polarization gradient: exploring an original route for optical trapping and manipulation. *Optics Express*, *18*, 6008.
[9] Nikolova, L., & Todorov, T. (1984). Diffraction efficiency and selectivity of polarization holographic recording. *Optica Acta*, *31*, 579–588.

[10] Cloutier, S. G. (2005). Polarization holography: orthogonal plane-polarized beam configuration with circular vectorial photoinduced anisotropy. *J. Phys. D: Appl. Phys.*, *38*, 3371–3375.
[11] Nikolova, L., & Ramanujam, P. S. (2009). *Polarization Holography*, Cambridge University Press.
[12] Juodkazis, S., Matsuo, S., Murazawa, N., Hasegawa, I., & Misawa, H. (2003). High–efficiency optical transfer of torque to a nematic liquid crystal droplet. *Appl. Phys. Lett.*, *82*, 4657–4659.
[13] Murazawa, N., Juodkazis, S., & Misawa, H. (2005). Characterization of bipolar and radial nematic liquid crystal droplets using laser-tweezers. *J. Phys. D: Appl. Phys.*, *38*, 2923–2927.
[14] Barnett, S. M. (2002). Optical angular momentum flux. *J. Opt. B: Quantum Semiclass. Opt.*, *4*, S7–S16.
[15] Kurose, R., & Komori, S. (1999). Drag and lift forces on a rotating sphere in a linear shear flow. *J. Flu. Mech.*, *384*, 183.
[16] Bagchi, P., & Balachandar, S. (2002). Effect of free rotation on the motion of a solid sphere in linear shear flow at moderate Re. *Physics of Fluid*, *14*, 2719.
[17] Oerstele, B. (1998). *T. Bui. Dinh., Exp. Fluids*, *25*, 16.
[18] Asmolov, E. S. (1999). The inertial lift on a spherical particle in a plane Poiseuille flow at large channel Reynolds number. *J. Fluid Mech.*, *381*, 63.
[19] Rubinow, S. I., & Keller, J. B. (1961). The transverse force on a spinning sphere moving in a viscous fluid. *J. Flu. Mech.*, *11*, 447–459.
[20] Saffman, P. G. (1965). The lift on a small sphere in a slow shear flow. *J. Flu. Mech.*, *22*, 385.
[21] Cipparrone, G., Hernandez, R. J., Pagliusi, P., & Provenzano, C. (2011). Magnus force effect in optical manipulation. *Phys. Rev. A*, *84*, 015802.